CrossMark

Enhanced Mechanical Properties, Corrosion Behavior and Bioactivity of Ti-based Bulk Metallic Glasses with Minor Addition Elements

Feng-Xiang Qin[1,3] · Yang Zhou[1] · Chuan Ji[1] · Zhen-Hua Dan[2] · Guo-Qiang Xie[3] · Sen Yang[1]

Abstract In this research, corrosion behavior, mechanical properties and bioactivity of Ti–Zr–Cu–Pd–Sn bulk metallic glasses with minor addition of Au, Pt, Nb or Ta elements were investigated. The results revealed that minor additions of the elements were beneficial to enhancing mechanical properties and corrosion resistance of Ti-based bulk metallic glasses. Minor addition of the element (especially with Nb and Ta addition) results in the improvement in plastic deformation ability due to the existing of nanoparticles with a size smaller than 10 nm in glassy matrix, inhibiting the deformation of the shear bonds. Enrichments of Ti and Zr elements in oxide layer were responsible for high corrosion resistance. The bioactivity of Ti-based bulk metallic glasses was also investigated. The best combination of large plastic deformation ability, good corrosion resistance and bioactivity in $Ti_{40}Zr_{10}Cu_{33}Pd_{14}Sn_2Ta_1$ BMG was obtained.

KEY WORDS: Bulk metallic glass; Microstructure; Alloy design; Corrosion; Mechanical behavior; Biocompatibility

1 Introduction

Bulk metallic glasses (BMGs) as novel metallic materials were rapidly developed in the past decades because of unique properties compared with conventional polycrystalline alloys [1]. Ti-based BMGs are expected as one of the most important metallic materials in orthopedics and dental surgery due to their low Young's modulus, high fracture strength, excellent strength-to-weight ratio, good corrosion resistance and superior biocompatibility of titanium [1–4]. Recently, the developments of Ni-free Ti–Zr–Cu–Pd and Ti–Zr–Cu–Pd–Sn BMGs with high glass-forming ability (GFA) make it possible to create new-generation metallic biomedical materials with acceptable properties [5–10]. Usually, BMG materials catastrophically fracture once the main shear band initiates and propagates without any obstacle. Therefore, brittleness is believed as an intrinsic characterization for metallic glasses. The plastic deformation of BMGs can be induced by suppressing of the propagation of shear bands in BMG composites. The ductility can be improved by in situ or ex situ particles in so-called BMG composites [9–14]. That is, by fabrication of BMG composites, the brittle fracture can be changed in some cases [11]. Relatively, the in situ techniques are more convenient and easier in practical applications than ex situ ones. In situ formed BMG composites can be synthesized by annealing of glassy precursors [15] or designing a proper alloy composition to produce a glassy matrix with dispersed crystalline phases [9, 16, 17]. The dispersion of nanoparticles with an

✉ Feng-Xiang Qin
  fengxiangqin@njust.edu.cn

1 School of Materials Science and Engineering, Nanjing University of Science and Technology, Nanjing 210094, China

2 College of Materials Science and Engineering, Nanjing TECH University, Nanjing 210009, China

3 Institute for Materials Research, Tohoku University, Sendai 980-8577, Japan

appropriate size and proper volume fraction is beneficial to enhancing the ductility of BMGs.

On the other hand, as the biomedical materials, corrosion behavior in Cl ion-containing solution and bioactivity is extremely essential and important. Corrosion properties and acceptable lifetime are so important for metallic implanting materials that the metallic materials cannot be utilized before the evaluation is given in different environments. Additionally, the formation and growth rate of apatite with similar structure and composition as those of bones on metallic implants are usually regarded as a simple criterion in evaluating bioactivity of metallic implants. BMG materials are chemically inert because of their chemically and structurally homogeneous state. Therefore, bioactive treatment is not as easy as hydrothermal treatment for conventional Ti alloys [18]. A special two-step treatment including hydrothermal–electrochemical treatment followed by an immersion in Hanks' solution is effective to Ti-based BMGs [8]. In this study, corrosion behavior, mechanical properties and bioactivity of $Ti_{40}Zr_{10}Cu_{34}Pd_{14}Sn_2$ and $Ti_{40}Zr_{10}Cu_{33}Pd_{14}Sn_2M_1$ (M = Au, Pt, Nb or Ta) were investigated.

2 Experimental Procedure

The alloy ingots $Ti_{40}Zr_{10}Cu_{34}Pd_{14}Sn_2$ (defined as base alloy) and $Ti_{40}Zr_{10}Cu_{33}Pd_{14}Sn_2M_1$ (M: Au, Pt, Nb or Ta) were prepared by arc melting of the mixture of pure metals (>99.9 mass%) in an argon atmosphere. The BMG rods with a diameter of 2.5 mm were fabricated by injection casting into copper mold. The ribbon samples with 10 mm in width and 40 μm in thickness were fabricated by melt spinning method. Thermal stability was characterized by differential scanning calorimetry (DSC, TA Q100) and differential thermal analysis (DTA, TA Q600) with a heating rate of 20 K/min. The structure was examined by X-ray diffraction (XRD, RIGAKU 4200) with CuK_α radiation. The mechanical testing was performed by compression at room temperature with a strain rate of 5×10^{-4} s^{-1}. The cylindrical samples with 2.5 mm in diameter and 5 mm in height were used, and they were polished carefully to ensure parallelism. At least three specimens for each condition were tested for the reproducibility. The microstructure of the as-cast samples was investigated by high-resolution transmission electron microscopy (HREM, JEOL 2010). The samples for transmission electron microscopy (TEM) observation were prepared by the ion-milling method.

The corrosion behavior of melt-spun samples was evaluated by potentiodynamic polarization measurement in 0.144 mol/L NaCl solution at 310 K open to air. Here, the concentration of 0.144 mol/L Cl ion is the same as that in simulated body fluid. Electrochemical measurements were taken in a three-electrode cell using a platinum counter electrode and a saturated calomel reference electrode (SCE). Potentiodynamic polarization curves were measured with a sweeping rate of 1 mV/s after immersing the samples at open circuit potential for 600 s. The elemental analysis of the samples after immersion in 0.144 mol/L NaCl solution was conducted by using an X-ray photoelectron spectrometer (XPS, ShimadzuKratos, AXIS-Ultra DLD) with monochromatized Al K_α excitation (hv = 1486.6 eV).

The ribbon samples were treated by hydrothermal–electrochemical method in 1 mol/L NaOH solution at 90 °C for 2 h under a direct current density of 10 mA/cm^2. Then, the hydrothermal–electrochemical-treated samples were pre-calcified by soaking in saturated Na_2HPO_4 and saturated $Ca(OH)_2$ in turn for 4 h. Finally, the two-step pre-treated samples were immersed in Hanks' solution at 37 °C for different times to observe the consequential processes of nucleation and growth of apatite. The chemical composition of Hanks' solution (g/L) was 8.00 NaCl, 0.40 KCl, 0.35 $NaHCO_3$, 0.19 $CaCl_2\cdot2H_2O$, 0.09 $Na_2HPO_4\cdot7H_2O$, 0.20 $MgSO_4\cdot7H_2O$, 0.06 KH_2PO4 and 1.00 glucose. Morphologies of surface-treated samples and side surface for the fractured samples were investigated by scanning electron microscopy (SEM, QUANTA FEG 250) equipped with X-ray energy dispersive spectroscopy (EDS).

3 Results and Discussion

In Fig. 1, the XRD patterns of all ribbon samples show only one halo peak located at about 38°, indicating that the as-prepared samples are in glassy state. Figure 2a, b shows DSC and DTA curves of $Ti_{40}Zr_{10}Cu_{34}Pd_{14}Sn_2$ and $Ti_{40}Zr_{10}Cu_{33}Pd_{14}Sn_2M_1$ (M: Au, Pt, Nb or Ta) ribbons. The
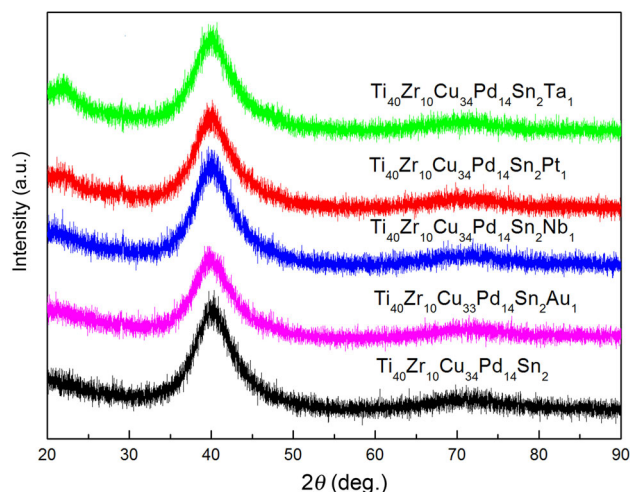

Fig. 1 XRD patterns of the Ti-based metallic glasses
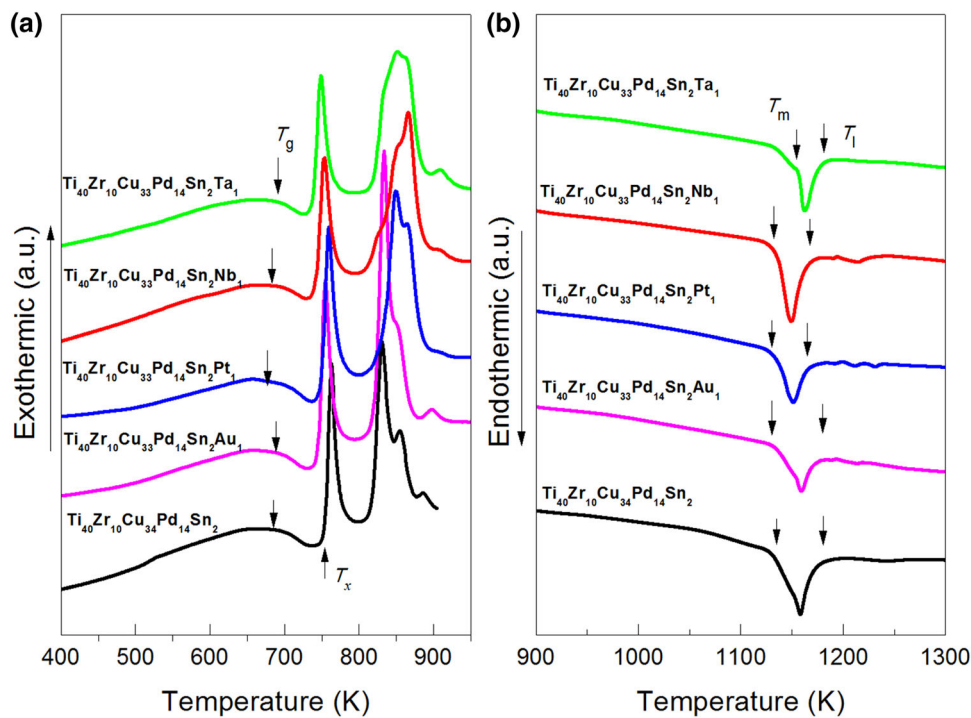
Fig. 2 DSC **a** DTA **b** curves of the Ti-based metallic glasses

glass transition temperature T_g and onset first-crystallization temperature T_x appear in all samples, followed by a multi-crystallization process. The onset melting temperature (T_m) and terminal melting temperature (T_l) are marked in Fig. 2b. To design and evaluate glass-forming ability (GFA) of BMGs, a number of parameters were reported to predict relative GFA of different multi-component alloy systems, such as the supercooled liquid (SCL) region (defined as $\Delta T_x = T_x - T_g$) [19], the reduced glass transition temperature T_{rg} ($T_{rg} = (T_g/T_m)$) [20] and the parameter γ ($\gamma = T_x/(T_g + T_l)$) [21]. In the present study, all the parameters of T_{rg}, ΔT_x and γ dependent on T_g, T_x, T_m or T_l are listed in Table 1. ΔT_x decreases with the addition of Au, Pt, Nb or Ta elements, indicating a little deteriorating of thermal stability. There is a little change in T_{rg} and γ, implying that the GFA is slightly influenced by the minor addition of Au, Pt, Nb or Ta, because T_{rg} and γ are stronger relevant to GFA than ΔT_x.

Corrosion behavior was investigated from the view of potential dynamic polarization testing for melt-spun samples. In 0.144 mol/L NaCl solution, all of the melt-spun samples are spontaneously passivated with a passive current density between 10^{-7} and 10^{-8} A/cm^2 (Fig. 3). The corrosion current densities are 2.02×10^{-8}, 1.80×10^{-8}, 1.70×10^{-8}, 1.30×10^{-8} and 0.65×10^{-8} A/cm^2 for the base alloy, 1% Au, 1% Pt, 1% Nb and 1% Ta addition BMGs, respectively. The corrosion potential was confirmed to be about -0.10 V for the base Ti$_{40}$Zr$_{10}$Cu$_{34}$Pd$_{14}$Sn$_2$ BMG, which shift slightly to positive position with the addition of Au, Pt, Nb or Ta. At the same time, the pitting potential increases with the addition of minor elements, located at 0.30–0.55 V. Elemental distribution of the oxide layers on melt-spun samples after immersion in NaCl solution for 168 h was analyzed by XPS. All of the designed elements were detected in partially oxidized state.

Table 1 Summary of T_g, T_x, T_m, T_l, ΔT_x ($T_x - T_g$), T_{rg} (T_g/T_m) and γ [$T_x/(T_g + T_l)$] for Ti$_{40}$Zr$_{10}$Cu$_{34}$Pd$_{14}$Sn$_2$ base alloy and Ti$_{40}$Zr$_{10}$Cu$_{33}$Pd$_{14}$Sn$_2$$M_1$ (M = Au(alloy I), Pt(alloy II), Nb (alloy III) or Ta(alloy IV)) BMGs

Alloy	T_g (K)	T_x (K)	T_m (K)	T_l (K)	ΔT_x (K)	T_{rg} (K)	γ (K)
Base alloy	693.2	754.0	1132.1	1172.9	60.8	0.61	0.400
Alloy I	695.3	744.4	1137.7	1171.1	49.1	0.61	0.399
Alloy II	699.4	749.0	1132.1	1165.5	49.6	0.61	0.402
Alloy III	693.2	743.4	1135.5	1161.4	50.2	0.61	0.400
Alloy IV	694.0	737.6	1153.7	1176.1	43.6	0.60	0.394
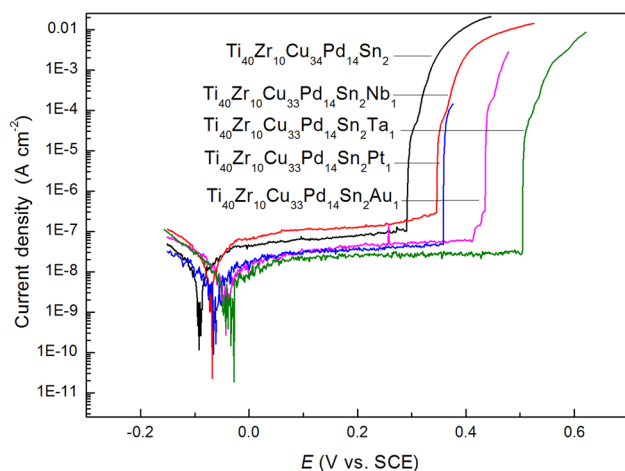
Fig. 3 Potentiodynamic polarization curves of the Ti-based metallic glasses in 0. 144 mol/L NaCl

Fig. 4 Compressive stress–strain curves of the Ti-based metallic glasses with a diameter of 2 mm

The relative contents of the metallic cations calculated from XPS spectra are listed in Table 2 after immersion in NaCl solution. The contents of Ti^{ox} and Zr^{ox} in outer layer are over 68 and 40%, which are much higher than the designed contents of 40 and 10%, respectively. Correspondingly, Cu^{ox} content is reduced lower than 4% for all the samples. The content of Pd^{ox} decreases from designed content of 14% to lower than 8.44%, accompanying with Sn element keeping almost stable.

Figure 4 shows the compressive stress–strain curves of the as-cast $Ti_{40}Zr_{10}Cu_{34}Pd_{14}Sn_2$ and $Ti_{40}Zr_{10}Cu_{33}Pd_{14}Sn_2M_1$ (M = Au, Pt, Nb or Ta) rods with a diameter of 2.5 mm. High strength of about 2000 MPa and low Young's modulus of about 80 GPa have been observed in the stress–strain curves for all BMG samples. Plastic deformation strain of 1.8, 2.5, 4.0, 6.0 and 10.2% corresponding to serrated flow sections is obtained in the base BMG and 1% Au-, Pt-, Nb- and Ta-added BMGs, respectively. Here, the serrated flow is attributed to the propagation of narrow shear bands under the compressive stress. It is proposed that the distinct plastic strains of the minor element-added BMGs originate from the obstacles of nanoparticles in glassy matrix to shear mode

deformation. On the side surface image, a multitude of jagged and interdicted shear bands are observed, especially for the fracture edge of the 1% Ta-added BMGs, as presented in Fig. 5, which is consistent with the results of compressive strength testing.

To clarify the detailed microstructure and understand the deformation mechanism of all examined as-cast BMGs with a diameter of 2.5 mm, microstructure of BMG samples was analyzed by HREM. Figure 6a–d shows the HREM images and the corresponding selected area diffraction (SAD) patterns of the $Ti_{40}Zr_{10}Cu_{34}Pd_{14}Sn_2$, $Ti_{40}Zr_{10}Cu_{33}Pd_{14}Sn_2Pt_1$, $Ti_{40}Zr_{10}Cu_{33}Pd_{14}Sn_2Nb_1$ and $Ti_{40}Zr_{10}Cu_{33}Pd_{14}Sn_2Ta_1$ BMGs, respectively. For all the as-cast samples, there are some nanoparticles in the glassy matrix. In the image of $Ti_{40}Zr_{10}Cu_{34}Pd_{14}Sn_2$ base BMG, small amount of nano-crystals like structural fringes are seen, accompanying with two rings overlapping on the halo ring of glassy matrix. The nanoparticles with a size smaller than 10 nm are distributed in glassy matrix for all the minor addition of Au, Pt, Nb or Ta BMGs. The corresponding SAD pattern in the inset consists of a broad diffraction halo and several diffraction rings identified as cubic Pd_3Ti with crystal planes of (111), (200), (220) and (311).

The two-step treatment as reported in previous work was carried out in 1 mol/L NaOH solution to the examined Ti-based BMGs [8]. All the samples with different compositions exhibit good bioactivity, i.e., after pretreatments and immersion in Hanks' solution, bone-like apatite may nucleate and grow fast on the surface of examined Ti-based BMGs. Here, only the results of $Ti_{40}Zr_{10}Cu_{33}Pd_{14}Sn_2Ta_1$ metallic glass were shown for discussion. Figure 7a shows the surface morphologies of $Ti_{40}Zr_{10}Cu_{33}Pd_{14}Sn_2Ta_1$ metallic glass after hydrothermal–electrochemical treatment in 1 mol/L NaOH solution. A porous and network microstructure is seen on the surface of
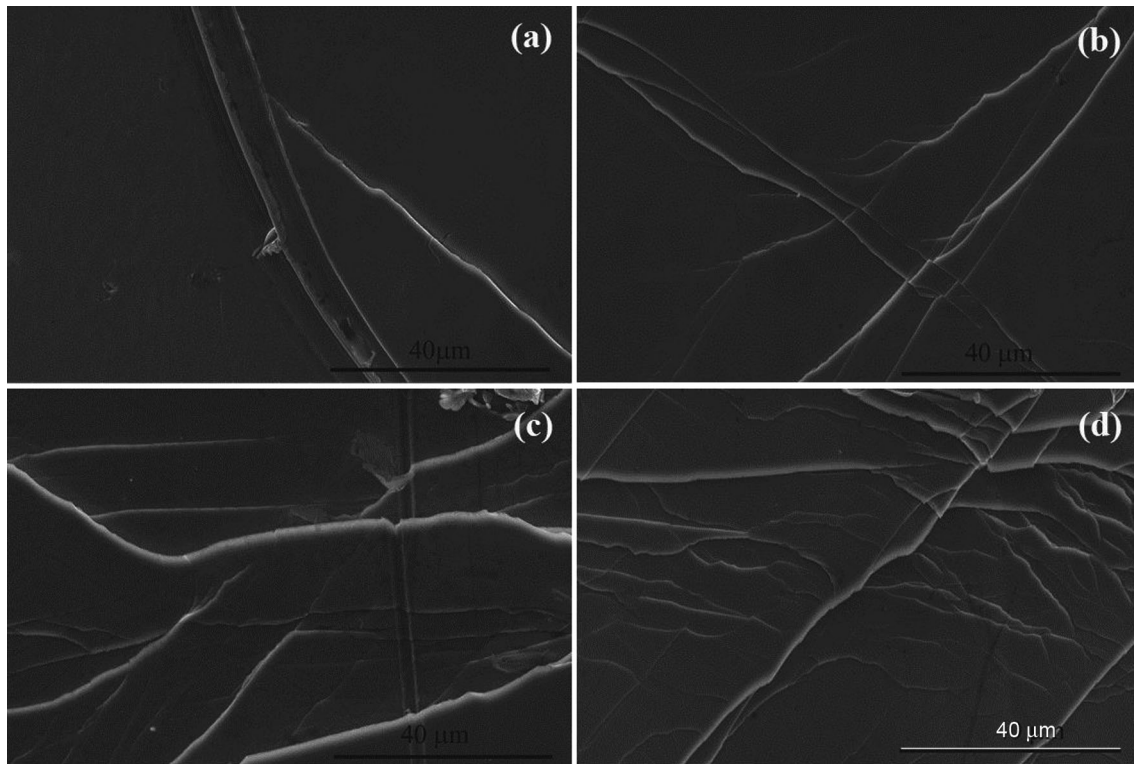
Table 2 Relative contents (atomic percent) of the surface metallic cations of $Ti_{40}Zr_{10}Cu_{34}Pd_{14}Sn_2$ and $Ti_{40}Zr_{10}Cu_{33}Pd_{14}Sn_2M_1$ (M: Au(Alloy I), Pt (Alloy II), Nb (Alloy III) or Ta (Alloy IV)) BMGs after immersion in NaCl solution

Alloy	Cu^{ox}	Ti^{ox}	Zr^{ox}	Pd^{ox}	Sn^{ox}	M^{ox}
Base alloy	0.63	70.39	19.26	8.44	1.28	
Alloy I	3.45	68.53	18.81	7.87	1.34	
Alloy II	1.83	70.18	19.50	7.29	1.20	
Alloy III	1.98	68.79	18.71	7.47	1.18	1.87
Alloy IV	0.29	71.01	19.45	7.43	1.02	0.80

Fig. 5 Side surfaces of the compressive facture samples of $Ti_{40}Zr_{10}Cu_{34}Pd_{14}Sn_2$ **a** $Ti_{40}Zr_{10}Cu_{33}Pd_{14}Sn_2Pt_1$ **b** $Ti_{40}Zr_{10}Cu_{33}Pd_{14}Sn_2Nb_1$ **c** $Ti_{40}Zr_{10}Cu_{33}Pd_{14}Sn_2Ta_1$ **d** BMGs with a diameter of 2.5 mm

$Ti_{40}Zr_{10}Cu_{33}Pd_{14}Sn_2Ta_1$ metallic glass enriched with Ti and O, as shown in Fig. 7b. Figure 7b, c shows the two-step pre–treated samples immersed in Hanks' solution at 37 °C for 1 and 4 days. After soaking in Hanks' solution for 1 day, a large amount of white particles are absorbed on the porous surface and parts of them connect each others (Fig. 7b), which are the nuclei of calcium phosphate compound [8]. Then, the layer grows and the Ca content increases with increasing immersion time. With further increasing in immersion time to 4 days, the Ca/P ratio reaches about 1.6 as shown in Fig. 7d, which is close to the ratio of Ca/P in apatite. Here, small amount of Mg and Na cations are also analyzed originating from Hanks' solution on the surface.

In this research, the influences of minor addition Au, Pt, Nb or Ta elements on the properties of Ti–Zr–Cu–Pd–Sn BMGs were studied. From the view of corrosion, high corrosion resistance has been obtained in 0.144 mol/L NaCl solution for the investigated Ti-based BMG. Destructive corrosion of the implants is usually induced by the aggressive Cl ion, which makes the implant loss the functions. Therefore, the concentration of 0.144 mol/L Cl ion is designed, which is equal to the concentration of Cl ion in simulated body fluid. XPS results demonstrate that the enrichments of Ti and Zr accompanying with the reduce of Cu in the oxide surface are responsible for the high ability

of spontaneous passivity. In other words, the protective layers mainly composed of Ti and Zr oxides cover the BMG substrates and protect the BMGs from corrosion although the attacking Cl ion exists. The addition of the elements, especially Nb or Ta element, further improves the pitting resistance by forming a protective oxide layer during the process of anodic polarization [22, 23].

As mentioned above, with the minor addition of Au, Pt, Nb or Ta, GFA of the Ti–Zr–Cu–Pd–Sn BMGs slightly decayed. The GFA of BMGs is related to the suppression of the formation of crystalline phases. In this research, Pd_3Ti nanoparticles with a particle size of several nanometers were observed in the glassy matrix due to the slightly deteriorating of GFA with minor addition elements. Consequently, the mechanical properties were also influenced by the precipitations. Actually, improvement of mechanical properties of BMG materials is a perpetual goal for the researchers since brittle fracture is an intrinsic character for BMGs. For biomedical materials, only the materials with proper mechanical properties and biocompatibility matching the requirements of metallic implants can be applied in clinic. Hence, the researchers are devoting to improving the plastic deformation ability of BMGs. Formation of an inhomogeneous structure with features, such as short-range or medium-range ordering clusters in glassy matrix, was considered to be in favor of enhancing plasticity of BMGs
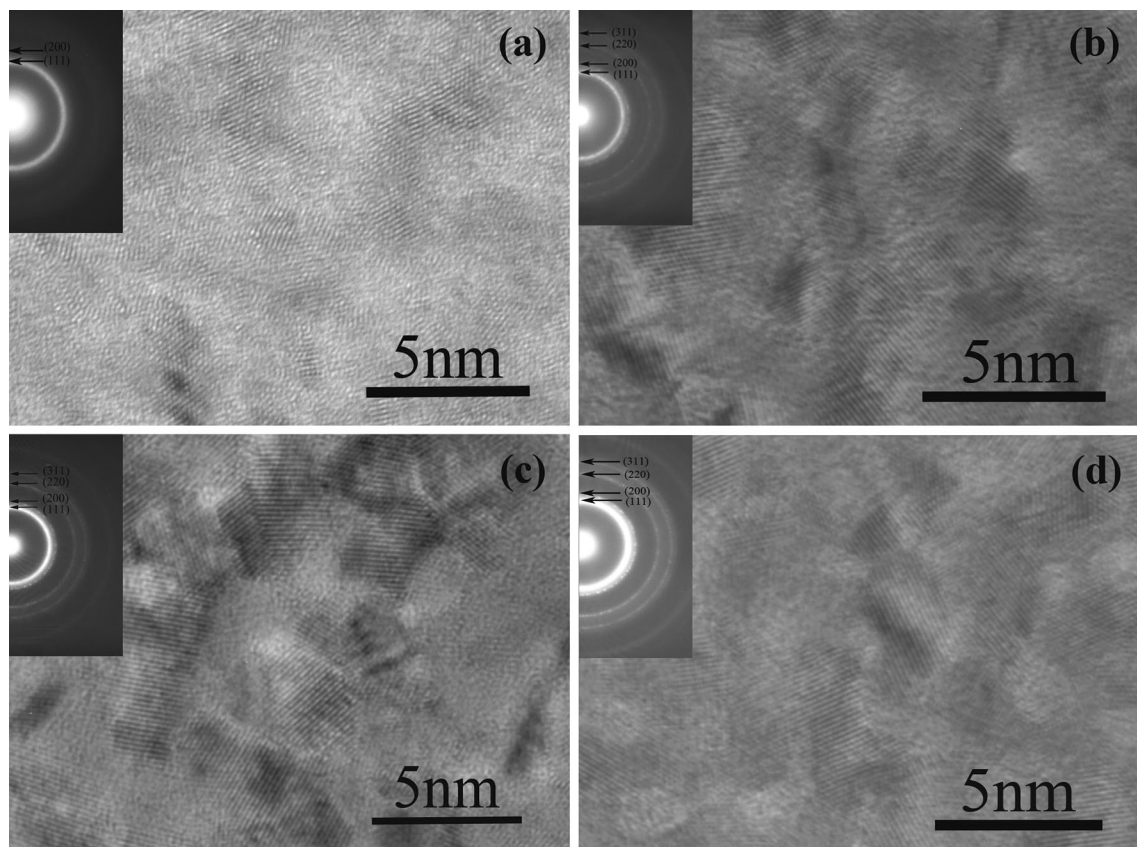
Fig. 6 HREM images and SADs of $Ti_{40}Zr_{10}Cu_{34}Pd_{14}Sn_2$ **a** $Ti_{40}Zr_{10}Cu_{33}Pd_{14}Sn_2Pt_1$ **b** $Ti_{40}Zr_{10}Cu_{33}Pd_{14}Sn_2Nb_1$ **c** $Ti_{40}Zr_{10}Cu_{33}Pd_{14}Sn_2Ta_1$ **d** BMGs with a diameter of 2.5 mm

[24, 25]. Moreover, in situ precipitation of ductile micrometer–sized particles or dendrites [26–28] has been produced by the addition of high melting point elements Ta, Nb or Mo, which is also effective to improve plastic deformation ability of BMGs. In this study, the large plastic deformation of the as-examined Ti-based BMGs is believed to originate from the mixed state of nanoparticles and glassy matrix. The phenomenon can be explained as follows. According to deformation mode of metallic glasses, local softening regions caused by temperature increasing under compressive process enhance the deformability [29]. In the case of the existence of nanoparticles, if the nanoparticles are much smaller than the shear bands, the deformation of the shear band is still dominated by the glassy matrix. Correspondingly, the nanoparticles act as the obstacles inhibiting the deformation of the shear bands [30]. Furthermore, from the view of the shear-transformation-zone theory [31], nanoparticles make the glassy matrix separate into a number of shear transformation zones. Within these shear transformation zones, local jammings relax easily results in the proceeding of the plastic deformation. Once the jammed state reaches a shear transformation zone, the system transforms into a continuously plastic deformation.

In Fig. 5, multiple shear bands were observed on the side surface of BMGs after compressive testing. The Pd_3Ti phase with small sizes hinders the propagation of the shear bands, leading to multiple shear bands in different directions. Therefore, plastic deformation was obtained for 1% Au-, Pt-, Nb- and Ta-added alloys, especially for the Nb– and Ta–added alloys. Beside the grain size, volume fraction of the precipitation phases is another dominating factor affecting plastic deformation behavior of BMGs, even if the dispersion of nanoparticles is beneficial to the improvement in ductility of BMGs [29, 31]. The difference in plastic strain of the several alloys might be triggered by the difference in particle size and volume fraction of nano-crystalline phases [15, 29].

On the other hand, the surface modification of Ti alloys is necessary to improve the bioactivity of implant–tissue osseointegration. TiO_2 layer on the surface of Ti alloys plays an important role in determining biocompatibility and corrosion behavior of Ti implant alloys. Simple hydrothermal treatment in alkali solution is not effective to Ti-based BMGs, because BMG materials exhibit high passivity ability [32]. In this research, the hydrothermal–electrochemical treatment at low temperature is suitable for
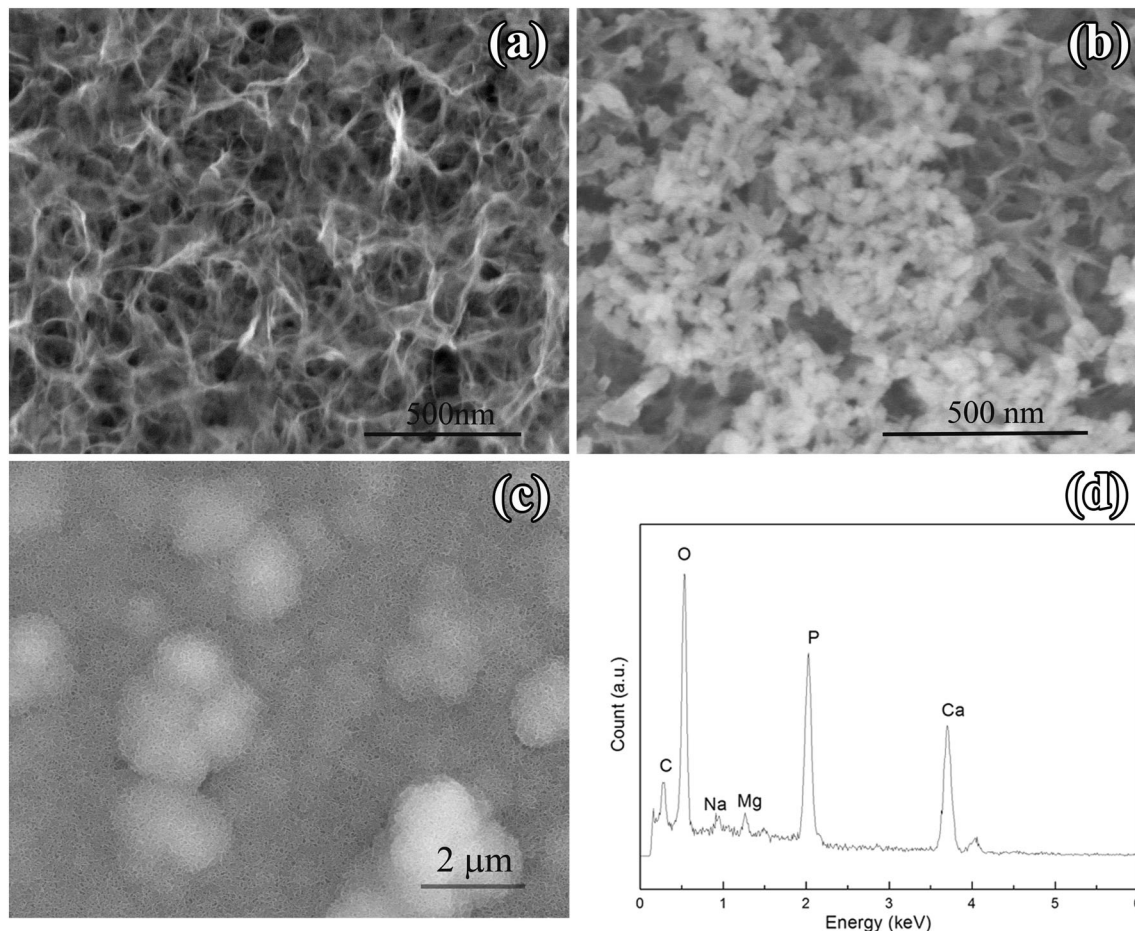
Fig. 7 SEM images and EDS results of the $Ti_{40}Zr_{10}Cu_{33}Pd_{14}Sn_2Ta_1$ metallic glass after hydrothermal–electrochemical treatment **a** immersion in Hanks' solution for 1 day **b** 4 days **c**, **d**

metallic glasses in the case of crystallization of them at high temperatures. It is known that hydrothermal–electrochemical treatment makes the negative charged layer of porous Ti oxide form in the outer surface, which exhibits good bioactivity [33, 34]. Consequently, to accelerate the nucleation of calcium phosphate, the pre-calcification procedure was carried out by soaking hydrothermal–electrochemical-treated Ti metallic glass in Na_2HPO_4 and $Ca(OH)_2$ in turn [35–39]. Pre-calcium treatment with high concentration of Ca^{2+} and HPO_4^{2-} accelerates the nucleation of calcium phosphate compounds in the following soaking in Hanks' solution. Finally, pre-treated samples were bathing in Hanks' solution to supply cations and anions for growth of apatite.

4 Conclusion

The effect of minor addition of Au, Pt, Nb or Ta element on corrosion, bioactivity and mechanical properties of $Ti_{40}Zr_{10}Cu_{34}Pd_{14}Sn_2$ BMGs was investigated. High yield strength of about 2000 MPa, low Young's modulus of about 80 GPa and distinct plastic strain of about 1.5–10.2% were achieved in 1% Au-, Pt-, Nb- or Ta-added Ti-based BMGs, due to the nanoparticles dispersed in the glassy matrix blocking the propagation of shear bands. High corrosion resistance of the Ti-based BMGs was obtained owing to the enrichment of Ti and Zr on the passive surface, and the corrosion resistance was improved with the minor additional elements, especially with the minor addition of Ta. Bone-like apatite formed on the Ti-based BMGs after hydrothermal–electrochemical pre-treatment and immersion in Hanks' solution. In this study, a good combination of good corrosion resistance, high strength accompanying with large plastic strain, and good bioactivity was obtained in Ti–Zr–Cu–Pd–Sn–Ta BMG, which exhibited high potential for the utilization as biomedical materials.

References

[1] A. Inoue, Acta Mater. **48**, 279 (2000)

[2] D. Cao, Y. Wu, H. Wang, X.J. Liu, Z.P. Lu, Acta Metall. Sin. (Engl. Lett.) **29**, 173 (2016)

[3] J.C. Qiao, J.M. Pelletier, J. Mater. Sci. Technol. **30**, 523 (2014)

[4] H.B. Ba, L.M. Dong, Z.Q. Zhang, D.S. Xu, R. Yang, Acta Metall. Sin. (Engl. Lett.) **29** (2016). doi: 10.1007/s40195-016-0443-9

[5] F.X. Qin, X.M. Wang, G.Q. Xie, S.L. Zhu, A. Kawashima, K. Asami, A. Inoue, Mater. Trans. **48**, 167 (2007)

[6] S.L. Zhu, X.M. Wang, F.X. Qin, A. Inoue, Mater. Sci. Eng. A **459**, 233 (2007)

[7] S.L. Zhu, G.Q. Xie, F.X. Qin, X.M. Wang, A. Inoue, Mater. Trans. **53**, 500 (2012)

[8] F.X. Qin, X.M. Wang, A. Inoue, Mater. Trans. **51**, 529 (2010)

[9] F.X. Qin, X.M. Wang, G.Q. Xie, A. Inoue, Intermetallics **6**, 1026 (2008)

[10] J.J. Oak, D.V. Louzguine-Luzgin, A. Inoue, J. Mater. Res. **22**, 1346 (2007)

[11] R. Wang, Y. Wang, J. Yang, J. Sun, L. Xiong, J. Non-Cryst. Solids **411**, 45 (2015)

[12] U. Kuhn, J. Eckert, N. Mattern, L. Schultz, Appl. Phys. Lett. **80**, 2478 (2002)

[13] C.H. Yim, W.L. Johnson, Appl. Phys. Lett. **71**, 3808 (1997)

[14] R. Busch, H.C. Yim, U. Koster, W.L. Johnson, Acta Mater. **47**, 2455 (1999)

[15] F.X. Qin, X.M. Wang, A. Inoue, Intermetallics **15**, 1377 (2007)

[16] J.C. Qiao, J.M. Pelletier, C. Esnour, Y. Liu, H. Kato, J. Alloy Compd. **607**, 139 (2014)

[17] J. Tan, F.S. Pan, Y. Zhang, W. Zhang, M. Stoic, B.A. Sun, U. Kuhn, J. Eckert, Mater. Sci. Eng. A **539**, 124 (2012)

[18] T. Kokubo, F. Miyaji, H.M. Kim, T. Nakamura, J. Am. Ceram. Soc. **79**, 1127 (1996)

[19] A. Inoue, Mater. Trans., JIM **36**, 866 (1995)

[20] Z.P. Lu, H. Tan, Y. Li, S.C. Ng, Scr. Mater. **42**, 667 (2000)

[21] Z.P. Lu, C.T. Liu, Acta Mater. **50**, 3501 (2002)

[22] S.J. Pang, T. Zhang, K. Asami, A. Inoue, J. Mater. Res. **18**, 1652 (2003)

[23] C.L. Qin, W. Zhang, K. Asami, H. Kimura, X.M. Wang, A. Inoue, Acta Mater. **54**, 3713 (2006)

[24] J. Li, X. Xu, T.C. Hufnagel, Microsc. Microanal. **9**, 509 (2003)

[25] T.C. Hufnagel, S. Brennan, Phys. Rev. B **67**, 014203-1-8 (2003)

[26] C. Fan, R.T. Ott, T.C. Hufnagel, Appl. Phys. Lett. **81**, 1020 (2002)

[27] J.C. Lee, Y.C. Kim, J.P. Ahn, H.S. Kim, S.H. Lee, B.J. Lee, Acta Mater. **52**, 1525 (2004)

[28] G. He, J. Eckert, W. Loser, L. Schultz, Nat. Mater. **2**, 33 (2003)

[29] L.Q. Xing, C. Bertrand, J.P. Dallas, M. Cornet, Mater. Lett. **34**, 90 (1998)

[30] K. Dasa, A. Bandyopadhyay, Y.M. Gupta, Mater. Sci. Eng. A **394**, 302 (2005)

[31] J.S. Langer, Scr. Mater. **54**, 375 (2006)

[32] F.X. Qin, X.M. Wang, T. Wada, G.Q. Xie, K. Asami, A. Inoue, Mater. Trans. **50**, 605 (2009)

[33] H.B. Wen, J.R. Wijn, F.Z. Cui, K. Groot, J. Biomed. Mater. Res. **41**, 227 (1998)

[34] A.H. Heuer, D.J. Fink, V.J. Laraia, J.L. Arias, P.D. Calvert, K. Kendall, G.L. Messing, J. Blackwell, P.C. Rieke, D.H. Thompson, A.P. Wheeler, A. Veis, A.I. Calpan, Science **255**, 1098 (1992)

[35] A.K. Shukla, R. Balasubramaniam, Corros. Sci. **48**, 1696 (2006)

[36] H.B. Wen, J. Brink, J.R. Wijn, F.Z. Cui, K. Groot, J. Cryst. Growth **186**, 616 (1998)

[37] B. Feng, J.Y. Chen, S.K. Qi, L. He, J.Z. Zhao, X.D. Zhang, Biomaterials **23**, 173 (2002)

[38] X.J. Yang, R.X. Hu, S.L. Zhu, C.Y. Li, M.F. Chen, L.Y. Zhang, Z.D. Cui, Scr. Mater. **54**, 1457 (2006)

[39] S.L. Zhu, X.J. Yang, Z.D. Cui, J. Alloy Compd. **504**, S168 (2010)